

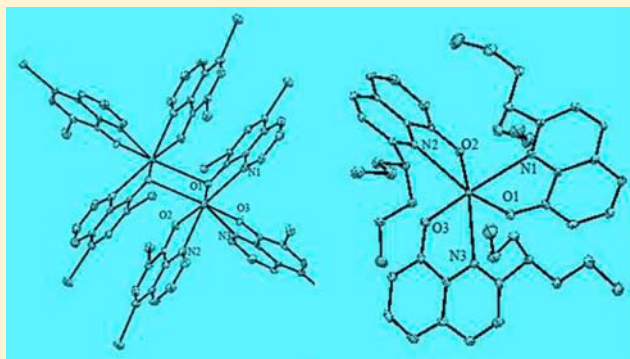
Luminescent Tris(8-hydroxyquinolates) of Bismuth(III)

Pauline J. Han, Arnold L. Rheingold,* and William C. Trogler*

Department of Chemistry and Biochemistry, University of California, San Diego, 9500 Gilman Drive, La Jolla, California 92093-0358, United States

Supporting Information

ABSTRACT: Luminescent homoleptic bismuth(III) complexes have been synthesized by adding several functionalized 8-hydroxyquinolate ligands to bismuth(III) chloride in a 3:1 mole ratio in either ethanol or tetrahydrofuran (THF) solvent. These complexes have been characterized by single-crystal X-ray diffraction (XRD) analysis, UV-vis spectroscopy, fluorescence spectroscopy, and density functional theory (DFT) calculations to determine their structures and photophysical properties. Reversible dimerization of the mononuclear tris(hydroxyquinolate) complexes was observed in solution and quantified using UV-vis spectroscopy. The fluorescence spectra show a blue shift for the monomer compared with homoleptic aluminum(III) hydroxyquinolate compounds. Four dimeric compounds and one monomeric isomer were characterized structurally. The bismuth(III) centers in the dimers are bridged by two oxygen atoms from the substituted hydroxyquinolate ligands. The more sterically hindered quinolate complex, tris(2-(diethoxymethyl)-8-quinolinato)bismuth, crystallizes as a monomer. The complexes all exhibit low-lying absorption and emission spectral features attributable to transitions between the HOMO (π orbital localized on the quinolate phenoxide ring) and LUMO (π^* orbital localized on the quinolate pyridyl ring). Excitation and emission spectra show a concentration dependence in solution that suggests that a monomer-dimer equilibrium occurs. Electronic structure DFT calculations support trends seen in the experimental results with a HOMO-LUMO gap of 2.156 eV calculated for the monomer that is significantly larger than those for the dimers (1.772 and 1.915 eV). The close face to face approach of two quinolate rings in the dimer destabilizes the uppermost occupied quinolate π orbitals, which reduces the HOMO-LUMO gap and results in longer wavelength absorption and emission spectral features than in the monomer form.



INTRODUCTION

Luminescent organometallic complexes containing heavy metals have been studied for their ability to harvest both triplet and singlet excitation in organic light-emitting diodes (OLEDs).¹⁻¹¹ OLEDs are attractive for use in flat-panel displays because they have a low operational voltage and simple fabrication, and possess a high brightness and efficiency.^{12,13} Luminescent metal complexes containing Pt(II) and Ir(III) have been shown to be highly efficient OLED emitters because their heavy-atom centers facilitate efficient energy harvesting through enhanced intersystem crossing.^{1-4,6-11,13-15} Another advantage of metal complexes as emitters is the ability to tune their emission energies through ligand substitution.¹⁰ Aluminum tris-8-hydroxyquinolinato (AlQ₃) has been a prototypical electroluminescent metal complex and is commercially used in OLEDs.⁵ By ligand substitution, it is possible to tune the emitting wavelength throughout the visible spectrum.¹⁶ The search for improved luminescent materials continues in order to improve the lifetime of OLED displays.¹⁶

Some factors that influence hydroxyquinoline (Q) ligand fluorescence include aromaticity, substitution on the aromatic ring, and structural rigidity.^{5,17} An increase in rigidity often leads to a decrease in nonradiative decay and increased

fluorescence. A high Z atom with greater spin-orbit coupling may enhance intersystem crossing (ICS), thereby increasing the likelihood of phosphorescence from the lowest excited state.¹⁸ Additionally, the type of metal-ligand bonding affects the emission energy of metal complexes. In hydroxyquinolate metal complexes, where emission often originates from a ligand-centered π - π^* transition, a metal-ligand bond with a more covalent character will shift the emission toward longer wavelength. Conversely, an ionic metal-ligand bond tends to result in an emission shifted toward shorter wavelength.⁵

In AlQ₃ complexes, it is generally thought that the lowest excited states involve π - π^* transitions centered on the 8-quinolate ligand that involve a net transfer of π -electron density from the phenoxide ring to the pyridyl ring.^{19,20} Molecular orbital calculations show that the highest occupied orbitals are filled π -orbitals of the quinolate phenoxide ring, whereas the lowest lying unfilled orbitals are quinolate π^* localized on the pyridyl side of the fused ring system.^{15,21} Free 8-hydroxyquinolate ligands do not normally emit strongly because of a low-lying nonradiative n - π^* transition that involves the phenoxide

Received: July 17, 2013

Published: October 4, 2013

oxygen lone pair.²² Metal coordination to the phenoxide oxygen raises the energy of this transition, so that the lowest excited state now becomes an emissive ligand-centered $\pi-\pi^*$ transition. Several trends have been noted for AlQ_3 complexes regarding ligand substitution. One example is that electron-donating groups on the C-5 and C-7 positions cause a red shift in absorption and emission wavelengths. Substitution at the C-4 or C-2 positions causes a red shift with electron-withdrawing groups and a blue shift with electron-donating groups.⁵

Heavy-metal complex emitters are being explored in radiation sensing applications using plastic scintillators to avoid limitations in fabrication of large area detectors posed by hard inorganic materials and liquid scintillators. Radiation sensing is crucial for the detection of illicit nuclear weapons material, detection of toxic radionuclides potentially used in "dirty bombs", and other national security applications. New materials that improve efficiencies of scintillators are needed to increase the radiation tolerance and maintain a high light output and transparency over several years.²³ A desirable formulation for a plastic scintillator generally contains a plastic base, a fluor, and a high-Z component. The base usually contains an aromatic group attached to a polymer backbone, such as polystyrene, while the dissolved fluor is an organic or inorganic emitter.²⁴ Organic fluorophores trap singlet excitons but can have increased efficiency through triplet-triplet annihilation,²⁵⁻²⁸ whereas heavy-metal emitters can trap both singlet and triplet excitons and increase the efficiency of plastic scintillators by as much as 3-fold.^{14,23,24} A high-Z component metal is also desirable to enhance the cross-section for interaction with γ -rays in radiation sensors.^{23,29,30} This study focuses on bismuth metal chelates that offer the potential for a high-Z emitting component in plastic scintillators. Bismuth is a low cost element and is the highest Z nonradioactive metal. It also exhibits relatively low toxicity for a heavy metal. For example, bismuth salicylate is used in stomach remedy preparations such as Pepto-Bismol.³¹⁻³⁵ For radiation sensing purposes, it is also desirable that the high-Z component fluor be highly soluble in organic scintillation polymers.^{24,30} The luminescent component should also possess a wide band gap that is unable to interfere with the aryl polymer scintillation mechanism.^{36,37}

At present, relatively few luminescent complexes of bismuth(III) are known.³⁷ This study reports the synthesis of new homoleptic bismuth(III) complexes with functionalized 8-hydroxyquinolate ligands. The ligands are either mono- or disubstituted with differing electron-withdrawing or -donating properties. The structures and luminescent behaviors of the monomeric and dimeric complexes formed with bismuth(III) are characterized.

EXPERIMENTAL METHODS

The 5-chloro-8-hydroxyquinoline and 8-hydroxy-2-methylquinoline ligands were purchased from Alfa Aesar, 5-chloro-8-hydroxy-7-iodoquinoline and 7-iodo-8-hydroxyquinoline-5-sulfonic acid were purchased from TCI America, 5,7-dichloro-8-hydroxyquinoline, 5,7-diiodo-8-hydroxyquinoline, 8-hydroxy-5-nitroquinoline, 7-bromo-8-hydroxyquinoline, and bismuth(III) chloride were purchased from Sigma-Aldrich, 8-hydroxyquinoline-2-carboxaldehyde was purchased from Acros Organics, and 8-hydroxyquinoline was purchased from EMD Chemicals Inc. Dry THF was purchased from Aldrich Chemical Co. Inc. and used after purification in an MBraun Auto Solvent Purification System using a dry nitrogen gas atmosphere. Spectroscopic grade dichloromethane (CH_2Cl_2) and N,N' -dimethylformamide (DMF) were purchased from Sigma-Aldrich and used for spectro-

scopic measurements. All other reagents were purchased from Sigma-Aldrich and used as received. Synthetic procedures were carried out using standard Schlenk techniques with a dry argon gas atmosphere.

Elemental combustion analyses were performed by Numeqa Resonance Laboratories, Inc., for C, H, and N. Fluorescence emission and excitation spectra were recorded with the use of a Perkin-Elmer spectrometer LS-50. Emission spectra were measured for four of the compounds in degassed CH_2Cl_2 at high and low concentrations at 298 K. These solutions were degassed with argon for 20 min. After admission of air, the color of the solutions did not change and the emission spectra did not show a noticeable quenching, indicating that dioxygen does not significantly quench emission in the bismuth(III) hydroxyquinolate compounds. Electronic absorption spectra were obtained with the use of a Perkin-Elmer Lambda 35 UV-vis spectrometer. NMR data were collected with the use of either a JEOL 500 MHz spectrometer or a Varian 400 MHz spectrometer and analyzed with JEOL Delta software. All measurements were taken at ambient temperature.

Tris(5-chloro-8-hydroxyquinolinato)bismuth (1). Bismuth(III) chloride (0.50 g, 1.60 mmol) was dissolved in dry ethanol (60.0 mL) in a round-bottom flask under an argon atmosphere at room temperature and stirred. After dissolution into a clear solution, 5-chloro-8-hydroxyquinoline (0.85 g, 4.8 mmol) was added to the stirring mixture. The reaction was refluxed for 3 h under an argon atmosphere. The solution turned dark yellow and was cooled to room temperature. Triethylamine and deionized water (10 mL) were added to neutralize the HCl produced, and a light yellow precipitate formed that was vacuum filtered and washed with ethanol (2×30 mL), deionized water (2×30 mL), and diethyl ether (2×30 mL). The compound was vacuum-dried and recrystallized by dissolving it in warm THF (323 K), filtering, and cooling to room temperature. The recrystallized material was dried under vacuum. This process was repeated once more and yielded a bright yellow colored powder (1.09 g, 92%). Anal. Calcd. for $C_{27}H_{15}BiCl_3N_3O_3$: C, 43.54; H, 2.03; N, 5.64. Found: C, 43.05; H, 2.03; N, 6.50.

Tris(5,7-dichloro-8-hydroxyquinolinato)bismuth (2). Compound 2 was obtained in a similar manner as 1 from bismuth(III) chloride (0.473 g, 1.5 mmol) and 5,7-dichloro-8-hydroxyquinoline (0.963 g, 4.5 mmol) in ethanol (60 mL). Triethylamine and deionized water (10 mL) were added to neutralize the HCl produced and precipitate the crude compound. Compound 2 was recrystallized from warm THF (323 K) after cooling to room temperature. The purification process was performed twice and produced a yellow-orange powder that was dried under vacuum (1.16 g, 92%). Anal. Calcd. for $C_{27}H_{12}BiCl_5N_3O_3$: C, 38.24; H, 1.43; N, 4.95. Found: C, 38.21; H, 1.43; N, 4.88.

Bis(μ^2 -5,7-diiodo-8-hydroxyquinolinato)tetra(5,7-diiodo-8-hydroxyquinolinato)dibismuthine 2.5-Tetrahydrofuran (3). Compound 3 was prepared in a similar manner as 1 from bismuth(III) chloride (0.315 g, 1 mmol) and 5,7-diiodo-8-hydroxyquinoline (1.19 g, 3 mmol) in ethanol (60 mL). Triethylamine and deionized water (10 mL) were added to neutralize the hydrochloric acid produced and to precipitate crude compound. The compound was recrystallized from warm THF (323 K) and precipitated by cooling to room temperature to yield dark orange crystals (1.24 g, 89%). Anal. Calcd. for $C_{64}H_{44}Bi_2I_{12}N_6O_{8.5}$: C, 25.85; H, 1.49; N, 2.83. Found: C, 23.13; H, 1.02; N, 3.22.

Bis(μ^2 -5-chloro-7-iodo-8-hydroxyquinolinato)tetra(5-chloro-7-iodo-8-hydroxyquinolinato)dibismuthine 3-Dichloromethane (4). Compound 4 was prepared in a similar manner as 1 from bismuth(III) chloride (0.315 g, 1 mmol) and 5-chloro-7-iodo-8-hydroxyquinoline (0.916 g, 3 mmol) in ethanol (60 mL). Triethylamine and deionized water (10 mL) were added to neutralize the HCl produced and precipitate crude compound. The crude powder was dried under vacuum. Anal. Calcd. for $C_{54}H_{16}Bi_2Cl_4I_6N_6O_6$: C, 29.02; H, 0.72; N, 3.76. Found: C, 29.28; H, 1.08; N, 3.70. It was further purified by dissolving in CH_2Cl_2 and filtering before layering with warm hexanes (343 K). Light brown crystals suitable for structural analysis were formed and collected by filtration (0.802, 71%).

Bis(μ^2 -7-bromo-8-hydroxyquinolinato)tetra(7-bromo-8-hydroxyquinolinato)dibismuthine 2-Tetrahydrofuran (5). Compound 5 was prepared in a similar manner as 1 from bismuth(III) chloride (0.315 g, 1 mmol) and 7-bromo-8-hydroxyquinoline (0.627 g, 3 mmol) in ethanol (60 mL). Triethylamine and deionized water (10 mL) were added to neutralize the HCl produced and precipitate crude compound. The crude product was purified by layering warm hexanes (343 K) over a THF solution. This yielded dark orange crystals (0.430 g, 49%) after drying in vacuo. Anal. Calcd. for $C_{31}H_{23}BiBr_3N_3O_4$: C, 39.16; H, 2.44; N, 4.42. Found: C, 35.44; H, 1.72; N, 4.83.

Tris(2-(diethoxymethyl)-8-quinolinato)bismuth (6). Compound 6 was prepared in a similar manner as 1 from bismuth(III) chloride (0.315 g, 1 mmol) and 8-hydroxy-2-quinoline-carboxaldehyde (0.520 g, 3 mmol) in ethanol (60 mL). Triethylamine and deionized water (10 mL) were added to neutralize the HCl produced and precipitate 6. The crude product was purified by dissolving it in THF and layering with warm hexanes (343 K). This yielded bright orange crystals (0.519 g, 55%). Anal. Calcd. for $C_{42}H_{48}BiN_3O_9$: C, 53.20; H, 5.11; N, 4.43. Found: C, 52.44; H, 5.31; N, 4.44.

Tris(8-hydroxy-2-methylquinolinato)bismuth (7). Compound 7 was prepared in a similar manner as 1 from bismuth(III) chloride (0.315 g, 1 mmol) and 8-hydroxy-2-methylquinolate (0.478 g, 3 mmol) in ethanol (60 mL). The reaction mixture was refluxed for 8 h. Triethylamine and deionized water (10 mL) were added to neutralize the HCl produced and precipitate 7. The compound was reprecipitated from hot THF (323 K) to yield a white-yellow powder (0.512 g, 75%). Anal. Calcd. for $C_{30}H_{24}BiN_3O_3$: C, 52.72; H, 3.54; N, 6.15. Found: C, 50.66; H, 3.54; N, 6.24.

Tris(8-hydroxy-5-nitroquinolinato)bismuth (8). Compound 8 was prepared in a similar manner as 1 from bismuth(III) chloride (0.315 g, 1 mmol) and 8-hydroxy-5-nitroquinolinol (1.19 g, 3 mmol) in ethanol (60 mL). Triethylamine and deionized water (10 mL) were added to neutralize the HCl produced and precipitate 8. The filter cake was dried under vacuum and yielded a bright yellow powder (0.781 g, 67%). Anal. Calcd. for $C_{27}H_{15}BiN_3O_9$: C, 41.77; H, 1.95; N, 10.82. Found: C, 41.27; H, 1.81; N, 10.69.

Triethylammonium Bis(μ^2 -7-iodo-8-hydroxyquinolinato-5-sulfonate)tetra(7-iodo-8-hydroxyquinolinato-5-sulfonate)dibismuthinate 1-Ethanol (9). Bismuth(III) chloride (0.315 g, 1 mmol) was dissolved in 60 mL of degassed THF at room temperature and stirred under an argon atmosphere. 7-Iodo-8-hydroxyquinoline-5-sulfonic acid (1.05 g, 3 mmol) was added quickly to the stirring mixture under argon. The yellow solution was refluxed for 3 h under argon and then cooled to room temperature. The sulfonic acid groups were neutralized with the addition of triethylamine and then recrystallized by slow evaporation. This yielded bright yellow-orange crystals (0.887 g, 70%). Anal. Calcd. for $C_{94}H_{132}Bi_2I_6N_{12}O_{26}S_6$: C, 35.09; H, 4.13; N, 5.22. Found: C, 32.80; H, 4.06; N, 5.10.

Tris(8-hydroxyquinolato)bismuth (10). Compound 10, which was reported previously,³⁷ was prepared in a similar manner as 1 from bismuth(III) chloride (0.315 g, 1 mmol) and 8-hydroxyquinoline (0.435 g, 3 mmol) in ethanol (60 mL). Triethylamine and deionized water (10 mL) were added to neutralize the HCl produced and precipitate 10. The compound was recrystallized from hot THF (323 K) and through slow evaporation yielded small bright green crystals (0.552 g, 86%). Anal. Calcd. for $C_{27}H_{18}BiN_3O_3$: C, 50.56; H, 2.83; N, 6.55. Found: C, 46.65; H, 3.50; N, 6.36.

Single Crystal X-ray Diffraction Analyses. All crystals were mounted on Cryo-loops with Paratone-N oil. Data for each sample were collected at 100 K with Mo $K\alpha$ radiation and corrected for absorption with the Siemens area-detector absorption correction program (SADABS). Data for compounds 3, 4, and 5 were collected with a Bruker Photon100 (CMOS) detector, while data for 9 was collected with a Bruker APEX II detector. For all samples, structures were solved by direct methods (SHELXTL), all non-hydrogen atoms were refined by full-matrix least-squares on F^2 , and all hydrogen atoms were placed in calculated positions with appropriate riding parameters. Solvent disorder was found for compounds 4 and 9. For 4, one chlorine atom on two of the CH_2Cl_2 solvent molecules was disordered and was refined using a two part (0.38/0.62 and 0.17/0.83) model. For

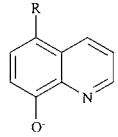
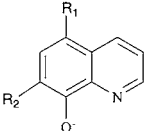
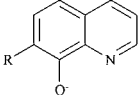
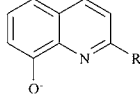
5, unrefined and diffused solvent THF molecules were treated using the PLATON program SQUEEZE. The use of restraints in the refinement of these structures involves solely the modeling of disordered solvent. SQUEEZE was used to render the solvent disorder in 5, and the details are reported in the CIF file. Data collection parameters for crystals are given in Table S1, Supporting Information.

Computational Methods. Density functional theory (DFT) calculations were performed with the Amsterdam Density Functional (ADF) program suite, version 2012.01, using the triple ζ Slater-type orbital basis set. Zero-order regular approximation (ZORA) was included for relativistic effects in conjunction with the local density approximation of Vosko et al.³⁸ Generalized gradient approximations for electron exchange and correlation were used as described by Becke and Perdew.³⁹ Molecular orbitals and final geometries were visualized with ADF-GUI.

RESULTS AND DISCUSSION

Bismuth(III) trisquinolates (BiQ_3) were prepared by adding $BiCl_3$ to 3 equiv of the respective 8-hydroxyquinoline ligands (Scheme 1) in either ethanol or tetrahydrofuran solvent and

Scheme 1. Compound Numbering Scheme for BiQ_3 Compounds

Ligand, Q	Compound Number (R)
	Compound 1 (R = -Cl) Compound 8 (R = -NO ₂)
	Compound 2 (R ₁ , R ₂ = -Cl) Compound 3 (R ₁ , R ₂ = -I) Compound 4 (R ₁ = -Cl; R ₂ = -I) Compound 9 (R ₁ = -SO ₃ H; R ₂ = -I)
	Compound 5 (R = -Br)
	Compound 6 (R = -C(OEt) ₂) Compound 7 (R = -CH ₃)

refluxing under an argon atmosphere. Aqueous triethylamine was then added to the reaction in order to neutralize the HCl produced on metathesis of $BiCl_3$ with the 8-hydroxyquinoline ligand and precipitate product.

Compound 9 was prepared in THF solvent because the free ligand is insoluble in ethanol. After vacuum filtration and subsequent drying under vacuum for 24–48 h, compounds with an approximate BiQ_3 stoichiometry were obtained in each case. With the exception of 3 and 8, the compounds were moderately soluble in common polar and aromatic solvents (including chloroform, CH_2Cl_2 , ethyl acetate, THF, and toluene) and insoluble in hydrocarbons (pentanes and hexanes). Compounds 3 and 8 were insoluble in all of the

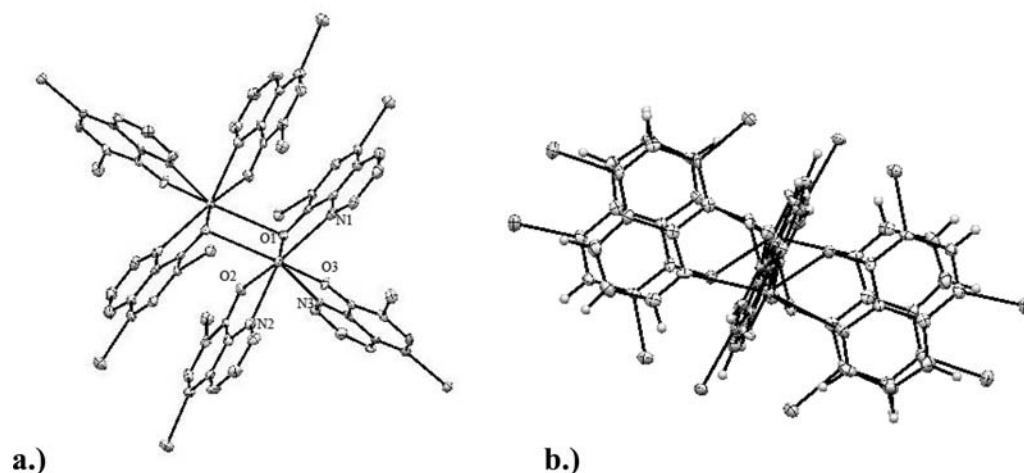


Figure 1. (a) ORTEP representation of compound 3. Probability ellipsoids are drawn at the 50% level. For clarity, lattice THF is omitted. (b) Plot showing eclipsed π -stacking of the quinolate rings when viewed from above the plane of the quinolate rings in the dimer along with a different view of the monomer. Only one of the crystallographically independent dimers is shown.

above solvents; however, all compounds were soluble in the polar donor solvent DMF. Compounds 1, 2, and 8 formed yellow powders on recrystallization from warm THF and layering with hexanes. Compound 7 formed a pale yellow powder after slow evaporation of THF solvent. Compounds 4 and 6 were recrystallized from THF/hexanes yielding dark brown and light yellow crystals, respectively. Compound 5 was recrystallized from CH_2Cl_2 /hexanes and formed large brown crystals. Compound 3 had moderate solubility when heated in THF. The hot solution was gravity filtered and crystallized by slow evaporation to yield dark orange crystals. Compound 9 was initially isolated in its protonated form from THF; however, the soft crystals obtained were amorphous by X-ray diffraction analysis. The compound was therefore recrystallized as the triethylammonium salt by the addition of triethylamine in THF solvent to deprotonate the sulfonic acid groups.

Emission spectra were observed for compounds 2, 4, 5, and 6 in degassed CH_2Cl_2 at high and low concentrations at 298 K. The emission spectra of degassed solutions did not show a noticeable change in intensity of the emission peaks, indicating that dioxygen does not efficiently quench their emission in solution.

Molecular Structures of BiQ_3 Compounds. Compounds 3, 4, and 5 all adopt a similar dimeric structure in the solid state. Compound 3 crystallizes with 2.5 molecules of lattice THF (Figure 1). Compound 5 crystallizes with one molecule of lattice THF solvent that is disordered. Compound 4 contains three molecules of dichloromethane in the formula unit. Selected bond lengths and angles of compounds 3–6 and 9 are reported in Tables 1 and 2.

Compounds 3, 4, and 5 all possess crystallographic inversion symmetry, and for compounds 4 and 5, there are two independent but structurally similar dimers in the unit cell.

In these compounds, the metal center is seven-coordinate with an approximate pentagonal bipyramidal geometry around the bismuth(III) centers. It has been noted that if stereochemically active lone pairs are assumed to be present, the structure of many bismuth(III) compounds can be regarded as eight-coordinate with a distorted dodecahedral geometry.^{40–42} The $\text{Bi}(1)\text{--N}(1)$ bond to the “axial” ligand on each bismuth is significantly shorter (2.335–2.364 Å) compared with the other $\text{Bi}\text{--N}$ bonds (2.582–2.603 Å). This most likely arises because

Table 1. Selected Bond Distances (Å) in Compounds 3–6 and 9

bond	3	4	5	6	9
$\text{Bi}(1)\text{--O}(1)$	2.287	2.329	2.303	2.217	2.320
$\text{Bi}(1)\text{--O}(2)$	2.275	2.320	2.331	2.196	2.316
$\text{Bi}(1)\text{--O}(3)$	2.353	2.295	2.328	2.183	2.321
$\text{Bi}(1)\text{--brO}(1)^a$	2.867	2.859	2.879		2.960
$\text{Bi}(1)\text{--N}(1)$	2.584	2.590	2.585	2.624	2.514
$\text{Bi}(1)\text{--N}(2)$	2.603	2.582	2.603	2.666	2.536
$\text{Bi}(1)\text{--N}(3)$	2.364	2.352	2.335	2.591	2.346
$\text{Bi}(1')\text{--O}(1')$	2.324	2.322			
$\text{Bi}(1')\text{--O}(2')$	2.308	2.299			
$\text{Bi}(1')\text{--O}(3')$	2.310	2.306			
$\text{Bi}(1')\text{--brO}(1')$	3.018	2.920			
$\text{Bi}(1')\text{--N}(1')$	2.559	2.658			
$\text{Bi}(1')\text{--N}(2')$	2.637	2.587			
$\text{Bi}(1')\text{--N}(3')$	2.339	2.332			
$\text{Bi}(1)\cdots\text{Bi}(1)$	3.792	3.568	3.674		3.670
$\text{Bi}(1')\cdots\text{Bi}(1')$	3.674	3.604			

^abr denotes the long bond to the oxygen of the bridging quinolate ligand.

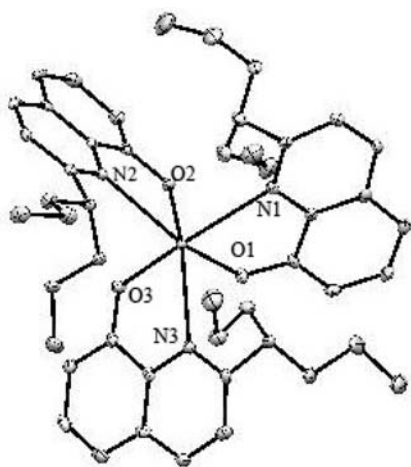
the axial quinolate ligand lies perpendicular to the other quinolate ligands in an environment with little steric crowding. The $\text{Bi}\text{--O}$ distances for the three quinolate ligands range between 2.275 and 2.331 Å. The bridging quinolates are asymmetric bridging groups with normal $\text{Bi}\text{--O}$ bond lengths to one bismuth(III) and a second significantly longer $\text{Bi}\text{--brO}$ distance at ~ 2.87 Å indicative of a weak bridging interaction between the monomers.

The dimer structures (e.g., right panel, Figure 1) show that the four equatorial quinolates (including the two nonbridging quinolate ligands) exhibit π -stacking so that the phenoxide rings eclipse the pyridyl rings. The HOMO in quinolates being a π -type orbital localized on the phenoxide portion of the hydroxyquinolate and the LUMO being a π -type orbital more localized on the pyridyl ring of the hydroxyquinolate ligand (*vide infra*) suggests a donor–acceptor π -interaction that may also contribute stability to the dimeric structure.

Table 2. Selected Bond Angles (deg) in Compounds 3–6 and 9

bond angle	3	4	5	6	9
O(1)–Bi(1)–O(2)	68.0	65.6	66.6	81.7	69.7
O(1)–Bi(1)–O(3)	130.4	137.3	134.1	87.7	131.8
O(2)–Bi(1)–O(3)	133.9	134.8	137.4	81.5	129.5
O(1)–Bi(1)–N(1)	67.0	66.2	67.1	67.8	67.6
O(2)–Bi(1)–N(1)	134.3	128.8	132.5	77.0	134.6
O(3)–Bi(1)–N(1)	74.7	76.5	74.3	117.2	73.6
O(1)–Bi(1)–N(2)	133.9	130.6	129.5	149.4	136.0
O(2)–Bi(1)–N(2)	67.2	66.2	65.9	67.8	67.7
O(3)–Bi(1)–N(2)	77.4	75.9	77.1	84.6	72.7
O(1)–Bi(1)–N(3)	77.1	79.7	79.8	72.1	74.6
O(2)–Bi(1)–N(3)	77.5	80.3	80.4	140.6	74.7
O(3)–Bi(1)–N(3)	69.6	70.9	70.9	68.8	70.2
N(1)–Bi(1)–N(2)	152.0	151.9	148.5	106.8	145.8
N(1)–Bi(1)–N(3)	85.5	75.0	81.9	117.2	82.6
N(2)–Bi(1)–N(3)	83.0	82.4	76.6	131.0	81.0
O(1)–Bi(1)–Bi(1)	48.9	53.1	51.6		53.7
O(2)–Bi(1)–Bi(1)	60.2	57.9	69.0		54.6
O(3)–Bi(1)–Bi(1)	165.9	163.4	162.4		172.7
N(1)–Bi(1)–Bi(1)	94.6	103.7	98.5		105.1
N(2)–Bi(1)–Bi(1)	113.3	107.0	112.6		109.1
N(3)–Bi(1)–Bi(1)	119.5	125.5	124.8		116.7

Tris(2-(diethoxymethyl)-8-quinolinato)bismuth (**6**) crystallizes as a monomer (Figure 2) with a six-coordinate metal center chelated by three quinolate ligands.

**Figure 2.** ORTEP representation of compound **6**. Probability ellipsoids are drawn at the 50% level.

The monomer structure approximates a trigonally distorted octahedral geometry with approximate C_3 symmetry and a *fac*-arrangement of the three hydroxyquinolate ligands. The metal center can be regarded as a seven-coordinate species with a stereochemically active lone pair extending along the C_3 axis toward the empty pocket formed by the acetal ligands, although electronic structure calculations (*vide infra*) do not indicate the presence of such an orbital. It should be noted that Al(III) quinolate complexes generally favor the meridional isomer,^{19,20,43,44} in contrast to the facial geometry found about bismuth(III). The relatively bulky substituent adjacent to N at the 2-position on the quinolate ring may enhance the stability of the monomer form in this case.

The expanded *cis*-N(1)–Bi–N(2) angles could be viewed as accommodating the bismuth lone pair but could also result from the relatively narrow bite of the chelate for the large Bi(III). The N(1)–Bi–N(2) bond angle expands to 106.84°, the N(3)–Bi–N(1) angle to 117.15°, and the N(3)–Bi–N(2) angle to 130.98°. The Bi–N bonds range between 2.591 and 2.666 Å, which are at the long end of typical ranges for Bi(III)–N bonds and suggestive of weak bonding.^{45–54} The three *cis*-oxygen bond angles concomitantly are decreased below 90° with the lengthening of the Bi–N bonds. The short Bi–O bonds and (2.183–2.127 Å) suggest strong ionic binding to the quinolate oxygens in the monomer. Crystal packing shows no close contact from other ligands; the closest atoms are separated by 3.972 Å.

The ionic compound triethylammonium tris(7-iodo-8-hydroxyquinolinato-5-sulfonate)bismuthate (**9**) also crystallizes as a dimer (Figure 3) similar to the structure of compounds **3**, **4**, and **5**. This compound contains three disordered triethylammonium cations per Bi(III) that counterbalance the charge of the anionic sulfonate substituents. There is also one disordered ethanol molecule of crystallization in the formula unit. The eclipsed π -stacking arrangement of the quinolate ligands is very similar to that in compounds **3**, **4**, and **5**, and the two halves of the dimer are related by an inversion center as in the other dimer structures. The weakly bridging ligand Bi–BrO contacts are 2.960 Å, which is significantly longer than the bridging Bi–O bonds (~2.87 Å) seen in the other dimers but similar to intrachain Bi–O oxygen contacts found in some Bi(III) alkoxide ladder polymers.⁵⁵ In **9**, the π -stacked quinolate ligands are splayed back slightly to minimize repulsive interactions between anionic sulfonate substituents on the 5-position of the quinolate ring, and this may account for the significantly lengthened Bi–O bridging distance in **9** compared with the other dimers. Bismuth(III) complexes that contain heteroatom donors with multiple lone pairs frequently expand their coordination shell and form dimers and oligomers in the solid state as observed here.^{45,52–73}

Crystallographic data and refinement information for the aforementioned compounds, along with ORTEP representations for compounds **4** and **5** is provided in Table S1 and Figures S1 and S2, Supporting Information.

Electronic Absorption Spectra. Absorption spectra were measured at several concentrations in 1 mm and 1 cm path length cuvettes (Figures S3–S9, Supporting Information) in either acetonitrile or CH_2Cl_2 . Compound **2** exhibits an absorption peak at 401 nm, which shows a deviation from Beer's law. Compound **3** displays similar behavior for the absorption peak at 400 nm. The absorption spectrum for compound **4** displays four peaks at 247, 305, 368, and 408 nm. The intensities of absorption peaks in compounds **2**–**10** did not follow Beer's law, which was most evident for the well-separated lowest energy absorption. For example, at the lowest concentrations of **5**, the 385 and 265 nm absorptions disappear (Figure 4), and both show a deviation from Beer's law with varying concentration (Table 3). Given the observation that the hydroxyquinolate complexes of bismuth(III) crystallize from solution as both monomeric and dimeric compounds, this suggests the presence of a solution equilibrium that shifts from the monomeric to the dimeric form at increasing concentrations.⁶⁰ The appearance of the new spectral features is attributed to those from the dimer form, which is held together by weak interactions, being dominant at higher concentrations. Concentration-dependent electronic spectra were obtained for

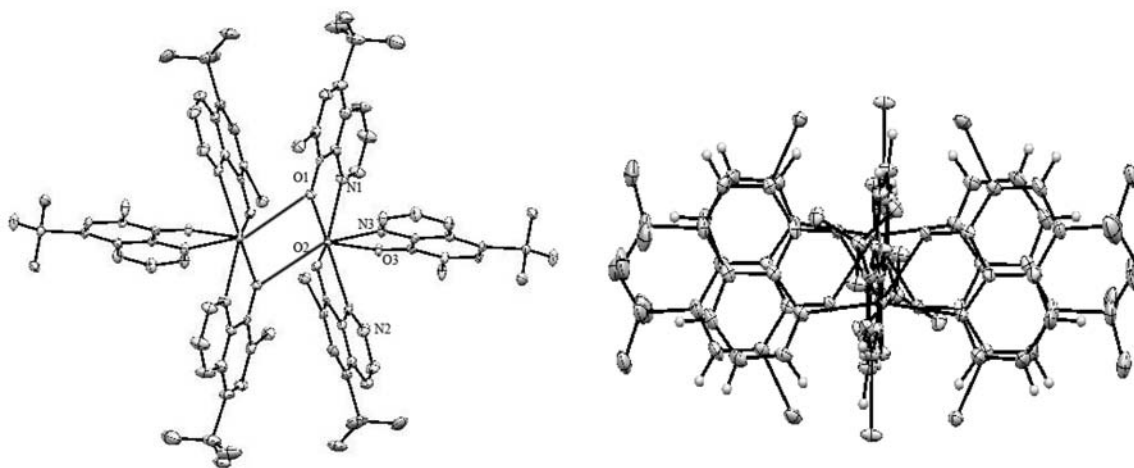


Figure 3. ORTEP representation of compound **9**. Probability ellipsoids are drawn at the 50% level. Lattice solvent and triethylammonium ions have been omitted for clarity. Right panel figure shows face to face overlap of quinolate rings in the dimer.

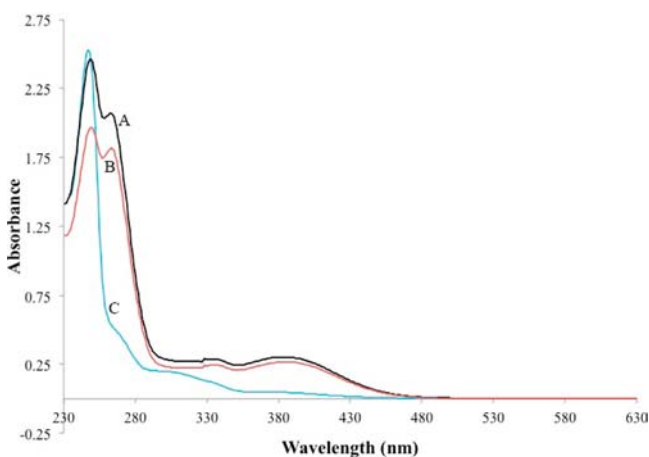


Figure 4. Electronic absorption spectra of **5** in CH_2Cl_2 at 298 K. (A) $[\mathbf{5}] = 2.16 \times 10^{-4}$ M, path length = 1 mm; (B) $[\mathbf{5}] = 1.26 \times 10^{-4}$ M, path length = 1 mm; (C) $[\mathbf{5}] = 1.54 \times 10^{-5}$ M, path length = 6.22 mm.²⁹

Table 3. Concentration-Dependent Absorbance Values for Compounds 5 (at 385 nm) and 6 (at 391 nm)

		concentration (M)	absorbance	ϵ ($\text{M}^{-1} \text{cm}^{-1}$)
5	A	2.16×10^{-4}	0.268	1400
	B	1.26×10^{-4}	0.267	2120
	C	1.54×10^{-5}	0.046	510
6	A	5.08×10^{-5}	0.164	530
	B	3.60×10^{-4}	0.326	900
	C	1.39×10^{-5}	0.0342	400

compounds **4**, **5**, and **7–10** (Tables S3–S8, Supporting Information) with similar results. Figure 5 shows the absorption spectra for **6**, which was found to be a monomer in the solid state. The new absorption peak that appears at 391 nm at higher concentrations shows that even a compound that prefers a monomeric form in the solid state exhibits spectral features suggestive of the monomer–dimer equilibrium in solution. The deviation from Beer's law at varying concentrations for compound **6** is shown in Table 3.

Monomer–Dimer Equilibrium. The deviations from Beer's law can be modeled as the monomer–dimer equilibrium shown in eq 1.

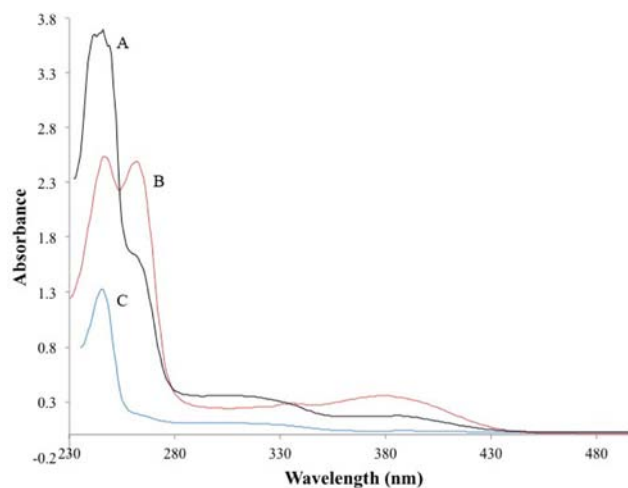


Figure 5. Electronic absorption spectra of **6** in CH_2Cl_2 at 298 K. (A) $[\mathbf{6}] = 5.08 \times 10^{-5}$ M, path length = 6.07 mm. (B) $[\mathbf{6}] = 3.60 \times 10^{-4}$ M, path length = 1 mm. (C) $[\mathbf{6}] = 1.39 \times 10^{-5}$ M, path length = 6.07 mm.



In eq 1, $[\text{BiQ}_3]_2$ is the dimeric form of BiQ_3 and Q is one of the ligands in **1–10**. The square root of absorbance was plotted against $[\text{BiQ}_3]/(\text{absorbance})^{1/2}$ in order to model this equilibrium.⁷⁴ Figure 6 illustrates the plots obtained for compounds **5** and **6**, which were a dimer and monomer, respectively, in the solid state. The conversion from monomer to dimer is modeled⁷⁴ by the following parameters: slope = $(2/\epsilon_2)$ and y intercept = $1/(\epsilon_2 K)^{1/2}$. The values found for ϵ_2 for the longest wavelength absorption band, and the equilibrium constant for dimer formation, K , for compounds **2–10** are given in Table 4. The modest value of these equilibrium constants, and the ability to readily observe both monomer and dimer forms in solution is consistent with the long weak bridging Bi–BrO bonds found in the solid state structures of the dimer form and the absence of a direct Bi–Bi bond.

Emission Spectra of Tris(hydroxyquinolato) Complexes of Bismuth(III). Tris-(8-hydroxyquinolato)aluminum (AlQ_3) displays a characteristic green emission and is commonly used as the electron transport and emitting layer in

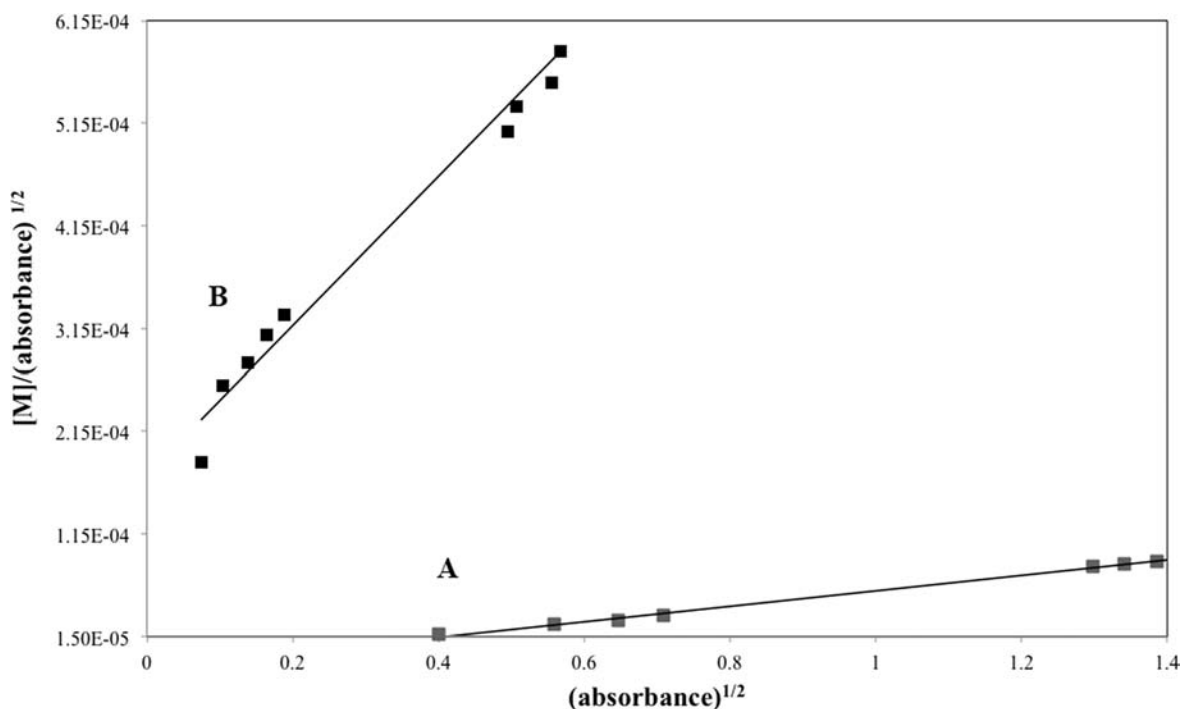


Figure 6. (a) Plot of $[5]/A_{385}^{1/2}$ vs $A_{385}^{1/2}$ over the concentration range from 1.082×10^{-4} to 7.008×10^{-6} M. The absorbance was measured in CH_2Cl_2 at 298 K and 385 nm. (b) Plot of $[6]/A_{391}^{1/2}$ vs $A_{391}^{1/2}$ over the concentration range from 2.07×10^{-4} to 1.34×10^{-5} M. The absorbance was measured in CH_2Cl_2 at 298 K and 391 nm.

Table 4. The ϵ_2 and K Values Derived from Fitting^a the Monomer–Dimer Equilibrium in Compounds 2–10

	2	3	4	5	6
ϵ_2	$(2.9 \pm 0.8) \times 10^3$	$(5.2 \pm 0.2) \times 10^2$	$(6.4 \pm 0.7) \times 10^3$	$(2.6 \pm 0.1) \times 10^4$	$(2.7 \pm 0.2) \times 10^3$
K	$(8.2 \pm 1.2) \times 10^4$	$(1.9 \pm 0.8) \times 10^5$	$(8.3 \pm 2.9) \times 10^4$	$(1.5 \pm 0.3) \times 10^5$	$(1.2 \pm 0.2) \times 10^4$
	7	8	9	10	
ϵ_2	$(1.4 \pm 0.1) \times 10^3$	$(2.5 \pm 0.1) \times 10^3$	$(2.8 \pm 0.1) \times 10^3$	$(1.5 \pm 0.1) \times 10^3$	
K	$(3.8 \pm 0.2) \times 10^5$	$(3.9 \pm 0.1) \times 10^4$	$(6.4 \pm 0.4) \times 10^5$	$(7.6 \pm 0.1) \times 10^6$	

^aFigure 6 and Figures S10–S16, Supporting Information.

low-molecular-weight OLEDs.²⁰ Molecular orbital studies have shown that the uppermost molecular orbitals are π -type and localized on the phenoxide ring of the quinolate ligand, while the lower unoccupied orbitals are π^* in character and more localized on the pyridyl ring. It was also observed that the lowest singlet state seen in absorption is a π - π^* transition primarily centered on the quinolate ligands.^{19,20,43,75} In AlQ_3 , the green emission band is centered at 556 nm.⁷⁶ The fluorescence spectra for tris(8-hydroxyquinoline)bismuth (BiQ_3) and **7** were examined previously and found to exhibit room temperature emission at 540 nm, as well as dual emission behavior noted for **7**.^{37,77} Emission features were assigned a ligand-localized fluorescence that is not associated with the heavy atom bismuth.

The emission spectra of all compounds in the present study were measured at room temperature. The compounds were first dried under vacuum for 24–48 h and added to their respective solvents. Table 5 summarizes the photophysical data for each compound. Compound **2** exhibits a single broad emission peak at 525 nm with a full width at half-maximum (fwhm) of 73 nm. According to Chen and Shi, the addition of halogen groups to the 5-position of the quinolinol ring will blue shift the emission of the compound.⁵ The addition of two chlorine groups on the 5- and 7-position of the 8-quinolate

Table 5. Absorption and Emission Spectral Data for Compounds 1–9 in Solution at Room Temperature

BiQ_3	λ_{max} nm (ϵ_{max} $\text{M}^{-1} \text{cm}^{-1}$)	λ_{max} nm (λ_{exc} nm)	Φ_f	solvent
1	246 (86600), 330 (10100)	423 (330)	<0.001	DMF
2	233 (11800), 271 (20600), 346 (4170)	525 (350)	0.0013	DMF
3	254 (112000), 353 (11900), 418 (14800)	371, 520 (354)	0.003	DMF
4	274 (65700), 350 (11700), 412 (11700)	393, 542 (352)	<0.001	DMF
5	246 (25450), 307 (1840), 385 (842)	390, 526 (354)	<0.001	DMF
6	253 (7220), 400 (597)	530 (350), 467 (240)	0.001	CH_2Cl_2
7	244 (62900), 299 (5640)	380	0.090	CH_2Cl_2
8	265 (36700), 348 (14400), 447 (82100)	484 (309)	0.001	DMF
9	273 (15800), 336 (9180), 379 (11500)	430 (351)	0.094	DMF

rings (**2**) follows this rule and slightly blue shifts the emission peak by 25 nm. The lowest absorption band of this compound can be similarly assigned a ligand centered π - π^* transition. The slightly blue-shifted emission observed for these compounds can be attributed to the π -electron donating ability

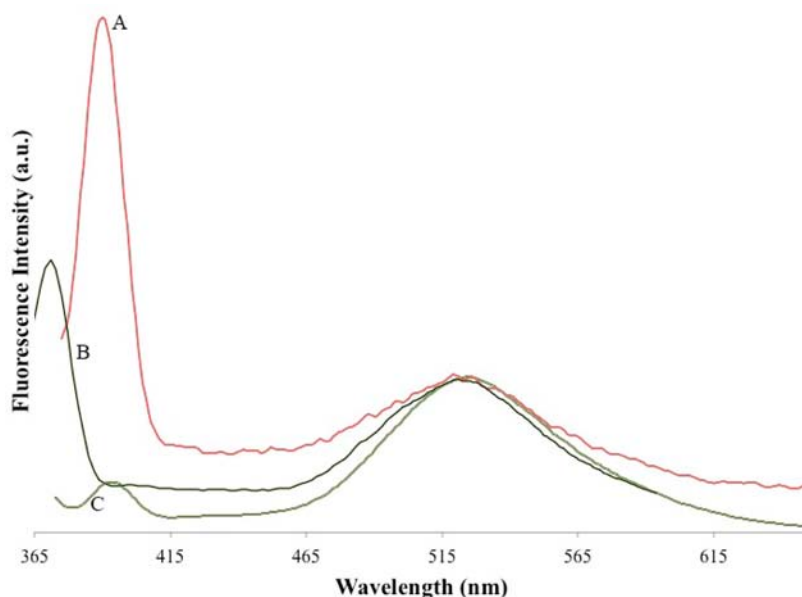


Figure 7. Emission spectra of (A) compound 5 at excitation wavelength 354 nm, (B) compound 3 at excitation wavelength 354 nm, and (C) compound 4 at excitation wavelength 352 nm. Spectrum A was taken in CH_2Cl_2 at 298 K; spectra B and C were taken in DMF at 298 K.

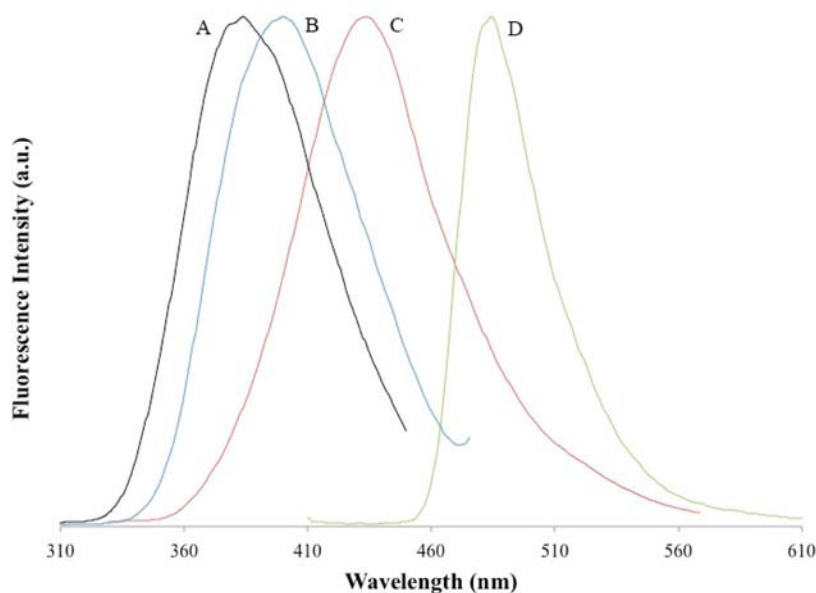


Figure 8. Emission spectra of (A) compound 6 with an excitation wavelength of 240 nm, (B) compound 1 with an excitation wavelength of 330 nm, (C) compound 9 with an excitation wavelength of 352 nm, and (D) compound 8, with an excitation wavelength of 309 nm. Spectrum A was taken in CH_2Cl_2 at 298 K. Spectra B, C, and D were taken in DMF at 298 K at lower concentrations where the monomer predominates.

of the halogen substituents in the 5- and 7-positions on the quinolate ligand.

The spectra (Figure 7) of compounds 3, 4, and 5 all show dual emission in solution. The higher energy emission feature is sharper and falls between 370 and 400 nm for the three compounds. The lower energy peak is broader and falls between 520 and 550 nm and exhibits fwhm of 78, 82, and 87 nm, respectively.

The lower energy emission feature in compound 3 is blue-shifted from BiQ_3 by 20 nm but remains in the green region of the spectrum. The emission can be assigned to the lowest ligand-centered $\pi-\pi^*$ transition similar to that seen previously in both AlQ_3 and BiQ_3 . For compounds 4 and 5, the lower energy emission features are blue-shifted by 8 and 20 nm,

respectively, from the BiQ_3 emission band. X-ray structural analysis shows that all three complexes have the ability to dimerize.

The emission spectra for 1, 6, 8, and 9 at room temperature are shown in Figure 8. These four compounds exhibit lowest energy emission peaks significantly blue-shifted from BiQ_3 . The emission peak of 6 is most shifted toward the blue. The large blue shift for 6 may result from its preferred monomeric structure. The long Bi–N bonds observed in 6 reflect decreased covalent bonding between the hydroxyquinolate nitrogen and the metal center, which is known to result in a large blue shift of the lowest energy $\pi-\pi^*$ (phenoxide \rightarrow pyridyl) transition of the quinolate ring.^{5,78,79} The molecular structure of the monomeric bismuth(III) compound shows a facial geometry.

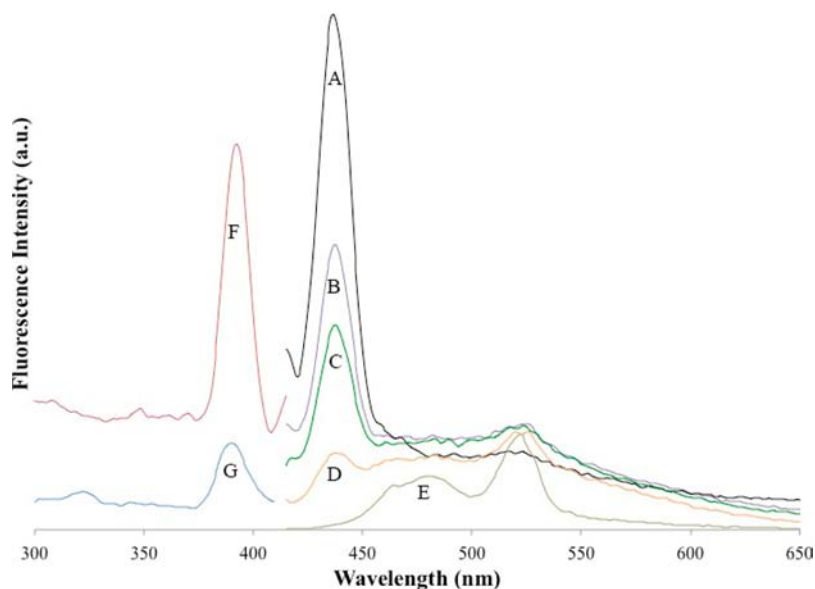


Figure 9. Emission (A–E) and excitation spectra (F, G) of **5** at increasing concentrations. (A, F) $[5] = 6.92 \times 10^{-6}$ M; (B) $[5] = 3.21 \times 10^{-5}$ M; (C) $[5] = 4.60 \times 10^{-5}$ M; (D) $[5] = 8.83 \times 10^{-5}$ M; (E, G) $[5] = 3.53 \times 10^{-4}$ M. Emission spectra were taken in CH_2Cl_2 at 298 K with excitation at 385 nm. Excitation spectrum G was monitored at an emission wavelength of 520 nm, while excitation peak F monitored the emission wavelength at 440 nm.

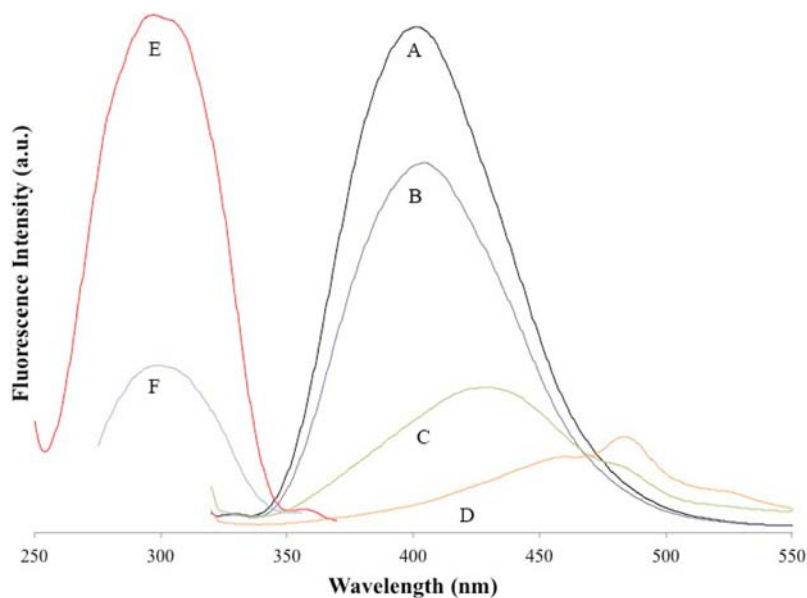


Figure 10. Solution emission (A–D) and excitation (E, F) spectra of **10** at varying concentrations. (A, E) $[10] = 3.32 \times 10^{-5}$ M; (B) $[10] = 4.29 \times 10^{-5}$ M; (C, F) $[10] = 1.46 \times 10^{-4}$ M; (D) $[10] = 2.58 \times 10^{-4}$ M. Emission spectra were taken in acetonitrile solvent with an excitation wavelength of 391 nm. Excitation spectra E and F monitored an emission wavelength at 518 nm, while excitation spectrum G used an emission wavelength at 497 nm.

This leads to unusually long Bi–N bond lengths in comparison to those found in the dimeric structures. The concentration-dependent dual emission observed in the other compounds can therefore be attributed to simultaneous emission by monomeric (shorter wavelength emission) and dimeric species (longer wavelength emission) both present in solution.

It has been noted that the HOMOs for hydroxyquinolate compounds are usually localized on the phenoxide ring, while the LUMOs are more localized on the pyridyl ring.⁸⁰ Due to their electron-withdrawing properties, the three substituents NO_2 , SO_3^- , and $-\text{C}(\text{OEt})_2$ may affect the distribution of π electron density of 8-hydroxyquinoline. The inductive influence

and resonance capabilities of NO_2 and SO_3^- also can act to stabilize the HOMO, thereby increasing the energy gap and promoting a blue shift in emission.⁸⁰ Delocalization of electrons from the phenoxide ring to the π -acceptor NO_2 or SO_3^- and can also alter the energy of the $n-\pi^*$ transitions, causing a further increase in energy for this type of transition.⁸¹

Emission Spectra at Varying Concentrations. Emission spectra were measured for **2**, **4**, **5**, and **6** at different concentrations (Figures S17–S20, Supporting Information) to observe whether oligomerization at higher concentrations altered the spectra because of a shift in the monomer–dimer equilibrium. Figure 9 shows the emission spectra at varying

concentrations for **5**. At lower concentrations (6.92×10^{-6} M), there is a prominent emission peak near 440 nm; at higher concentration (3.53×10^{-4} M), the dominant emission peak is at 520 nm. The spectra resemble corresponding concentration-dependent changes in the absorption spectra where the longest wavelength absorption at low concentrations is at 307 nm but at higher concentrations a 385 nm absorption appears.

Compound **6** exhibits a broad emission peak at 518 nm and another stronger emission band at 467 nm. Like the previous compounds at higher concentrations, the higher energy peak corresponding to the monomer decreases in relative intensity to the long wavelength emission (Figure S20, Supporting Information). The monomer emission peak in this complex is red-shifted compared with the monomer peaks in the other compounds. This could be partially due to the substituent on the pyridyl ring. The solid-state emission spectrum of this compound, which crystallizes as a monomer, does not exhibit the longer wavelength emission peak.

Additional results (Figures S17 and S18, Supporting Information) show that compound **2** exhibits mostly one broad emission band at 526 nm at higher concentrations and predominantly one emission band at 440 nm at lower concentrations. Because dimerization occurs at higher concentrations, the dimer form of **2** can be assigned to the lower energy emission peak, while the monomer is assigned the higher energy emission peak as for the preceding compounds. Similar behavior (Figure S19, Supporting Information) is shown by compound **4**.

In Figure 10, the emission spectra at varying concentrations (from 3.32×10^{-5} to 2.58×10^{-4} M) for the unsubstituted tris(8-hydroxyquinolato)bismuth (**10**) are shown. Previous studies reported³⁷ that **10** has one emission band at long wavelength (540 nm) at room temperature in solution, but the concentrations were not specified. Emission spectra for **10** show a similar concentration behavior to the other compounds studied here. At lower concentrations, **10** predominantly exhibits a high-energy emission (415 nm) characteristic of the monomer. At higher concentrations, new emission peaks emerge at lower energies consistent with a dimer being present.

The room temperature fluorescence quantum yields obtained (Table 5) for the bismuth(III) quinolates are relatively low as the weak interaction of Bi(III) with the ligand π system does not appear to alter intersystem crossing and enhance phosphorescence.⁷⁷ The blue shift in emission observed between the monomeric and dimeric forms of the Bi(III) compounds can be attributed to the very long bismuth to nitrogen bonds observed in the monomer. This suggests considerable ionic character with primary bonding of Bi(III) to the anionic quinolate oxygen. It is noted that boron tris(quinolate) compounds are solely bound to boron via oxygen and exhibit significantly blue-shifted emission spectra compared with transition metal quinolates.^{78,82} Chen and Shi also determined that decreasing covalent character in the metal–nitrogen bond results in a blue shift of the lowest quinolate electronic transitions.⁵ Not only does bismuth exhibit more ionic metal–ligand bonding character, but relatively long Bi–N bond lengths were observed in complexes **4**, **5**, **6**, and **9** by single-crystal X-ray diffraction analysis compared with the relatively short bond length from Bi(III) to the phenolate oxygens. Since it is accepted that as the metal–nitrogen bond length increases, emission tends to shift to a higher energy,^{5,78,79} the question remaining is why the dimeric form

of the compounds emit at longer wavelengths. DFT calculations were performed to address this question further.

Electronic Structure Calculations. To obtain a better understanding of the electronic structures of the mononuclear and dinuclear compounds, density functional theory (DFT) calculations were employed using the structural parameters for crystalline compounds **4**, **5**, and **6**.

The energy level diagrams (Figure 11) show qualitatively that in the monomer, the uppermost occupied orbitals are three

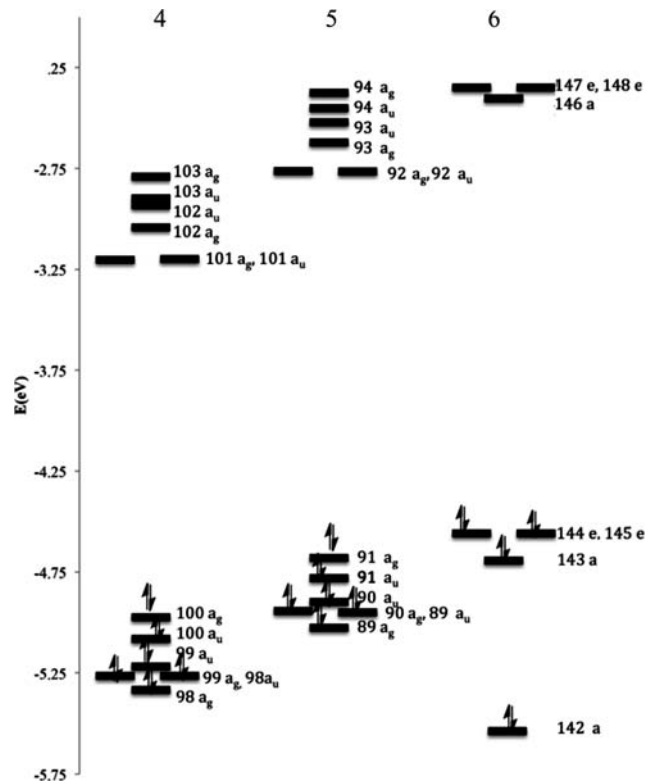


Figure 11. Energy level diagrams of frontier quinolate π orbitals of compounds **4**, **5**, and **6**.

quinolate ligand-centered π bonding orbitals localized more on the phenoxide ring. The lower unoccupied orbitals are the three corresponding π^* orbitals that are more localized on the pyridyl ring. In the dimer, the antibonding and bonding π orbitals are split and doubled because there are twice as many ligands. The six upper occupied orbitals are still quinolate ligand-centered π orbitals localized on the phenoxide ring, while the six lowest empty orbitals in the dimer are π^* quinolate orbitals localized on the pyridyl ring. The face-to-face overlap of the two pairs of quinolate rings in the dimer, however, broadens the energy range of the π and π^* orbitals and thereby reduces the HOMO–LUMO π – π^* gap. For example, in the dimers, the face-to-face π interaction should cause repulsion between the uppermost filled π orbitals and raise their energy. The uppermost occupied orbitals in the dimers are predominantly the equatorial quinolate π orbitals and their destabilization causes the decrease in the HOMO–LUMO gap. In addition, other excited state coupling effects, such as exciton splitting, could further shift and split or broaden the ligand localized π – π^* transition due to π -stacking of the quinolate ligands in the dimers as, for example, is observed for π – π^* transitions in π -stacked phthalocyanine complexes.⁸³

Table 6. Molecular Orbital Atomic Compositions (%) of Frontier π Orbitals in Compound 5^a

	Bi	Br	O _A	N _A	O _B	N _B	O _C	N _C
94 a _g				9.54		9.78		
94 a _u	4.4			18.35				
93 a _u	5.19					16.93		1.23
93 a _g	6.61			8.07		9.12		
92 a _g							2.14	16.26
92 a _u							2.09	16.09
91 a _g		8.05	10.02		15.6			
91 a _u		7.68	7.78		16.12	1.05		
90 a _u		4.56	13.32	1.18	3.4		4.09	
90 a _g		8.41					22.75	1.02
89 a _u		7.23					19.23	
89 a _g	1.36	6.01	11.17	1.55	6.21		1.85	

^aThe subscript A denotes atomic character from the nonbridging equatorial quinolate ligands, B denotes the bridging equatorial ligands, and C denotes the two terminal quinolates of the dimer.

The predominant atomic compositions of the frontier molecular orbitals are provided in Tables 6 and 7 for

Table 7. Molecular Orbital Atomic Compositions (%) of Frontier π Orbitals in Compound 6

	Bi	O	N
147 e	1.95	1.09	19.83
148 e	1.95	1.11	20.97
146 a	5.16		20.00
145 e		26.17	
144 e		25.46	
143 a	1.28	22.24	
142 a	11.96	35.60	21.09

compounds 5 and 6 for the heteroatom components of the π frontier orbitals that are associated with the hydroxyquinolate π system. Compounds 4 and 5 were calculated with idealized C_i symmetry, while 6 was calculated with an idealized C_3 geometry. The bismuth metal centers have only a minor contribution to the frontier orbitals in these compounds similar to Al(III) quinolate complexes. None of the uppermost occupied orbitals could be identified with a stereochemically active Bi lone pair. Even though this concept may be convenient to rationalize structural descriptions, there was no direct evidence for a nonbonding lone pair in the present calculations.

X-ray diffraction analysis has shown that 4 and 5 crystallize as dimers, with two of the quinolate ligands (L_A and L_B) on each Bi in a pseudoequatorial position and that the equatorial quinolates on opposing Bi atoms are stacked in an antiparallel eclipsed fashion. The final two quinolate ligands (L_C) in the dimer are pseudoaxial and lie perpendicular to equatorial ligands L_A and L_B . Ligand L_C , under density functional theory (DFT) analysis, contributes little to the HOMO/LUMO orbitals in the dimers. The calculated HOMO–LUMO energy gap in 4 is 1.772 eV (700 nm), and in 5 it is 1.915 eV (647 nm), which are reduced from the value found in the monomer 6 at 2.156 eV (575 nm). The decreased energy gap in the dimers qualitatively correlates with observed trends in the experimental emission and absorption peaks discussed previously.

For ligands L_A and L_B in the dimers (Table 6, Figure 12), the HOMO electron cloud is mostly π character and concentrated on the phenoxide rings. Similarly, the electron clouds of the

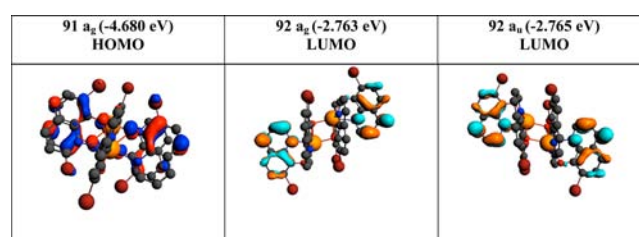


Figure 12. HOMO/LUMO molecular orbitals for compound 5.

LUMO are concentrated on the nitrogen and carbon atoms of the pyridyl ring and are mostly composed of π^* character. Occupied and unoccupied molecular orbitals for compound 4 are given in Table S9, Supporting Information.

The bismuth metal center is a minor contributor to frontier orbitals in all the compounds and there is no evidence for direct Bi–Bi bonding in the DFT calculations.

CONCLUSIONS

Ten substituted 8-hydroxyquinolates of bismuth(III) were prepared, and the compounds adopt monomeric and dimeric structures in solution and in the solid state. The monomer form BiQ_3 exhibits a facial orientation of the quinolate ligand that is different from the meridional isomer found in Al(III) and Ga(III) quinolate complexes. The dimeric structures form by asymmetric bridging of quinolate oxygens from two ligands approximately equatorial to the long nonbonding $\text{Bi}\cdots\text{Bi}$ axis of the dimer. The structure also appears to be stabilized by a donor–acceptor π -stacking interaction between the four equatorial quinolate ligands on adjacent Bi(III) so that the phenoxide ring of one quinolate lies above the pyridyl ring of the parallel quinolate ligand on the adjacent Bi(III). The ionic Bi–O bonding appears to be significantly stronger than the covalent Bi–N bonding to the hydroxyquinolate ligand in all the compounds based on the structural data.

Both UV–vis and photoluminescence spectra showed a blue shift of the monomer absorption spectrum compared with AlQ_3 . This is most likely due to extremely elongated bismuth–nitrogen bonds in the monomer, which reflects reduced covalent bonding between Bi(III) and the N atom of the pyridyl ring. Both absorption and photoluminescence spectroscopy showed that the compounds exhibit absorption and emission peaks the relative intensity of which varies with concentration and can be attributed to the presence of a

monomer–dimer solution equilibrium. Electronic structure calculations show that the monomer contained three uppermost π -bonding orbitals localized on the phenoxide ring, while the three lowermost unoccupied π -orbitals were localized on the pyridyl ring. The dimers exhibited a doubling and energy broadening of the frontier ligand π orbitals compared with the monomer. Face-to-face overlap of equatorial quinolate rings in the dimers further caused the energy broadening and reduced the HOMO–LUMO π – π^* gap. This can account for the lowered energy of absorption and emission peaks observed in the dimers. The heavy Bi(III) ion does not appear to enhance the efficiency of room temperature luminescence, as the quantum yields are low. The blue-shifted emission in the monomers, however, may offer an advantage in high band gap polymer scintillators compared with AlQ₃. Challenges remain to improve quantum yields by enhancing structural rigidity of the complexes and increasing the stability of the monomer form by the addition of rigid steric bulk at the 2-position of the quinolate ring.

■ ASSOCIATED CONTENT

■ Supporting Information

Crystallographic and refinement information, concentration-dependent extinction coefficients for **2**, **3**, **4**, **7**, **8**, **9**, and **10**, frontier molecular orbital atomic compositions for DFT calculation of **4**, ORTEP plots of compounds **4** and **5**, concentration-dependent electronic absorption spectra of **2**, **3**, **4**, **7**, **8**, **9**, and **10**, plots of monomer/dimer equilibrium determinations for **2**, **3**, **4**, **7**, **8**, **9**, and **10**, fluorescence spectrum for **2**, excitation spectrum and concentration-dependent fluorescence spectra for compounds **2**, **4**, and **6**, and ligand labels for DFT calculation of **4**. This material is available free of charge via the Internet at <http://pubs.acs.org>.

■ AUTHOR INFORMATION

Corresponding Author

*E-mail: wtroglar@ucsd.edu.

Notes

The authors declare no competing financial interest.

■ ACKNOWLEDGMENTS

This work was supported by the National Nuclear Security Administration, Office of Defense Nuclear Nonproliferation, Office of Nonproliferation Research and Development (NA-22) of the U.S. Department of Energy. Helpful discussions with Dr. Nerine Cherepy and Dr. Steven Payne (Lawrence Livermore National Laboratories) are gratefully acknowledged.

■ REFERENCES

- (1) Adachi, C.; Baldo, M. A.; Forrest, S. R.; Lamansky, S.; Thompson, M. E.; Kwong, R. C. *Appl. Phys. Lett.* **2001**, *78*, 1622–1624.
- (2) Adachi, C.; Baldo, M. A.; Forrest, S. R.; Thompson, M. E. *Appl. Phys. Lett.* **2000**, *77*, 904–906.
- (3) Adachi, C.; Baldo, M. A.; Thompson, M. E.; Forrest, S. R. *J. Appl. Phys.* **2001**, *90*, 5048–5051.
- (4) Burrows, P. E.; Sapochak, L. S.; McCarty, D. M.; Forrest, S. R.; Thompson, M. E. *Appl. Phys. Lett.* **1994**, *64*, 2718–2720.
- (5) Chen, C. H.; Shi, J. *Coord. Chem. Rev.* **1998**, *171*, 161–174.
- (6) Baldo, M. A.; Forrest, S. R.; Thompson, M. E. *Opt. Eng.* **2005**, *94*, 267–305.
- (7) Djurovich, P. I.; Thompson, M. E. *Highly Effic. OLEDs Phosphoresc. Mater.* **2008**, 131–161.
- (8) Forrest, S. R.; Burrows, P. E.; Thompson, M. E. *Laser Focus World* **1995**, *31*, 99, 101–102, 104, 106–107.

- (9) Forrest, S. R.; Burrows, P. E.; Thompson, M. E. *Chem. Ind.* **1998**, 1022–1026.
- (10) Ma, B.; Djurovich, P. I.; Thompson, M. E. *Coord. Chem. Rev.* **2005**, *249*, 1501–1510.
- (11) Thompson, M. E.; Lamansky, S.; Djurovich, P.; Murphy, D.; Abdel-Razzaq, F.; Forrest, S. R.; Baldo, M.; Burrows, P. E. *Polym. Mater. Sci. Eng.* **2000**, *83*, 202–203.
- (12) Utz, M.; Chen, C.; Morton, M.; Papadimitrakopoulos, F. *J. Am. Chem. Soc.* **2003**, *125*, 1371–1375.
- (13) Pfeiffer, M.; Forrest, S. R. *Nanoelectron. Inf. Technol.* **2003**, 915–931.
- (14) Baldo, M. A.; Thompson, M. E.; Forrest, S. R. *Nature* **2000**, *403*, 750–753.
- (15) Burrows, P. E.; Shen, Z.; Bulovic, V.; McCarty, D. M.; Forrest, S. R.; Cronin, J. A.; Thompson, M. E. *J. Appl. Phys.* **1996**, *79*, 7991–8006.
- (16) Montes, V. A.; Pohl, R.; Shinar, J.; Anzenbacher, P. *Chem.—Eur. J.* **2006**, *12*, 4523–4535.
- (17) Chen, Z.-F.; Song, X.-Y.; Peng, Y.; Hong, X.; Liu, Y.-C.; Liang, H. *Dalton Trans.* **2011**, *40*, 1684–1692.
- (18) Lytle, F. E.; Storey, D. R.; Juricich, M. E. *Spectrochim. Acta, Part A* **1973**, *29*, 1357–1369.
- (19) Gao, H.-Z.; Su, Z.-M.; Qin, C.-S.; Mo, R.-G.; Kan, Y.-H. *Int. J. Quantum Chem.* **2004**, *97*, 992–1001.
- (20) Halls, M. D.; Schlegel, H. B. *Chem. Mater.* **2001**, *13*, 2632–2640.
- (21) Jang, H.; Do, L.-M.; Kim, Y.; Zyung, T.; Do, Y. *Synth. Met.* **2001**, *121*, 1667–1668.
- (22) Popovych, O.; Rogers, L. B. *Spectrochim. Acta* **1959**, *15*, 584–592.
- (23) Rupert, B. L.; Cherepy, N. J.; Sturm, B. W.; Sanner, R. D.; Dai, Z.; Payne, S. A. *MRS Proc.* **2011**, 1341.
- (24) Rupert, B. L.; Cherepy, N. J.; Sturm, B. W.; Sanner, R. D.; Payne, S. A. *Europhys. Lett.* **2012**, *97*, 22002.
- (25) Sternlicht, H.; Nieman, O. C.; Robinson, O. W. *J. Chem. Phys.* **1963**, *38*, 1326–1335.
- (26) Carman, L.; Zaitseva, N.; Martinez, H. P.; Rupert, B.; Pawelczak, I.; Glenn, A.; Mulcahy, H.; Leif, R.; Lewis, K.; Payne, S. *J. Cryst. Growth* **2013**, *368*, 56–61.
- (27) Zaitseva, N.; Glenn, A.; Carman, L.; Hatarik, R.; Hamel, S.; Faust, M.; Schabes, B.; Cherepy, N.; Payne, S. *IEEE Trans. Nucl. Sci.* **2011**, *58*, 3411–3420.
- (28) Zaitseva, N.; Rupert, B. L.; Pawelczak, I.; Glenn, A.; Martinez, H. P.; Carman, L.; Faust, M.; Cherepy, N.; Payne, S. *Nucl. Instrum. Methods Phys. Res., Sect. A* **2012**, *668*, 88–93.
- (29) Shmurak, S. Z.; Kedrov, V. V.; Klassen, N. V.; Shakhrai, O. A. *Phys. Solid State* **2012**, *54*, 2266–2276.
- (30) Cherepy, N. J.; Payne, S. A.; Sturm, B. W.; Kuntz, J. D.; Seeley, Z. M.; Rupert, B. L.; Sanner, R. D.; Drury, O. B.; Hurst, T. A.; Fisher, S. E. Comparative gamma spectroscopy with SrI2 (Eu), GYGAG (Ce) and Bi-loaded plastic scintillators. *Nuclear Science Symposium Conference Record (NSS/MIC)*, 2010, 2012; IEEE: New York, 2012; pp 1288–1291.
- (31) Braunschweig, H.; Cogswell, P.; Schwab, K. *Coord. Chem. Rev.* **2011**, *255*, 101–117.
- (32) Freedman, L. D.; Doak, G. O. *Chem. Rev.* **1982**, *82*, 15–57.
- (33) Guo, Z.; Sadler, P. J. *Angew. Chem., Int. Ed.* **1999**, *38*, 1512–1531.
- (34) Sadler, P. J.; Li, H.; Sun, H. *Coord. Chem. Rev.* **1999**, *185*–186, 689–709.
- (35) Briand, G. G.; Burford, N. *Chem. Rev.* **1999**, *99*, 2601–2657.
- (36) Moser, S. W.; Harder, W. F.; Hurlbut, C. R.; Kusner, M. R. *Radiat. Phys. Chem.* **1993**, *41*, 31–36.
- (37) Ballardini, R.; Varani, G.; Indelli, M. T.; Scandola, F. *Inorg. Chem.* **1986**, *25*, 3858–3865.
- (38) Vosko, S. H.; Wilk, L.; Nusair, M. *Can. J. Phys.* **1980**, *58*, 1200–1211.
- (39) Becke, A. D. *Phys. Rev. A* **1988**, *38*, 3098–3100.

- (40) Hoffmann, R.; Beier, B. F.; Muetterties, E. L.; Rossi, A. R. *Inorg. Chem.* **1977**, *16*, 511–522.
- (41) Anjaneyulu, O.; Maddileti, D.; Kumara Swamy, K. C. *Dalton Trans.* **2012**, *41*, 1004–1012.
- (42) Lawton, S. L.; Fuhrmeister, C. J.; Haas, R. G.; Jarman, C. S.; Lohmeyer, F. G. *Inorg. Chem.* **1974**, *13*, 135–143.
- (43) Curioni, A.; Boero, M.; Andreoni, W. *Chem. Phys. Lett.* **1998**, *294*, 263–271.
- (44) DeMasi, A.; Piper, L. F. J.; Zhang, Y.; Reid, I.; Wang, S.; Smith, K. E.; Downes, J. E.; Peltekis, N.; McGuinness, C.; Matsuura, A. J. *Chem. Phys.* **2008**, *129*, No. 224705.
- (45) Stavila, V.; Davidovich, R. L.; Gulea, A.; Whitmire, K. H. *Coord. Chem. Rev.* **2006**, *250*, 2782–2810.
- (46) Hegetschweiler, K.; Stucky, S.; Morgenstern, B.; Neis, C.; Weyhermuller, T. *Acta Crystallogr.* **2009**, *C65*, m1–3.
- (47) Brechbiel, M. W.; Gansow, O. A.; Pippin, C. G.; Rogers, R. D.; Planalp, R. P. *Inorg. Chem.* **1996**, *35*, 6343–6348.
- (48) Le Bris, J.; Hubert-Pfalzgraf, L. G.; Daniele, S.; Vaissermann, J. *Inorg. Chem. Commun.* **2007**, *10*, 80–83.
- (49) Shimada, S.; Yamazaki, O.; Tanaka, T.; Suzuki, Y.; Tanaka, M. J. *Organomet. Chem.* **2004**, *689*, 3012–3023.
- (50) Bensch, W.; Reifler, F. A.; Reller, A.; Oswald, H. R. Z. *Kristallogr.* **1989**, *189*, 169–79.
- (51) Ranjbar, M.; Aghabozorg, H.; Moghimi, A. Z. *Kristallogr. - New Cryst. Struct.* **2003**, *218*, 432–434.
- (52) Stavila, V.; Whitmire, K. H. *Acta Crystallogr.* **2010**, *E66*, m1547–m1548.
- (53) Evans, W. J.; Rego, D. B.; Ziller, J. W. *Inorg. Chim. Acta* **2007**, *360*, 1349–1353.
- (54) Briand, G. G.; Burford, N. *Adv. Inorg. Chem.* **2000**, *50*, 285–357.
- (55) Bachman, R. E.; Whitmire, K. H.; Thurston, J. H.; Gulea, A.; Stavila, O.; Stavila, V. *Inorg. Chim. Acta* **2003**, *346*, 249–255.
- (56) Levason, W.; Reid, G. *Compr. Coord. Chem. II* **2004**, *3*, 465–544.
- (57) Jolas, J. L.; Hoppe, S.; Whitmire, K. H. *Inorg. Chem.* **1997**, *36*, 3335–3340.
- (58) Jones, C. M.; Burkart, M. D.; Bachman, R. E.; Serra, D. L.; Hwu, S. J.; Whitmire, K. H. *Inorg. Chem.* **1993**, *32*, 5136–44.
- (59) Jones, C. M.; Burkart, M. D.; Whitmire, K. H. *Angew. Chem.* **1992**, *104*, 466–467; *Angew. Chem., Int. Ed. Engl.* **1992**, *31* (4), 451–452.
- (60) Stavila, V.; Fettingner, J. C.; Whitmire, K. H. *Organometallics* **2007**, *26*, 3321–3328.
- (61) Thurston, J. H.; Marlier, E. M.; Whitmire, K. H. *Chem. Commun.* **2002**, 2834–2835.
- (62) Thurston, J. H.; Whitmire, K. H. *Inorg. Chem.* **2002**, *41*, 4194–4205.
- (63) Thurston, J. H.; Whitmire, K. H. *Inorg. Chem.* **2003**, *42*, 2014–2023.
- (64) Whitmire, K. H. *Chemtracts: Inorg. Chem.* **1995**, *7*, 167–181.
- (65) Whitmire, K. H.; Hoppe, S.; Sydora, O.; Jolas, J. L.; Jones, C. M. *Inorg. Chem.* **2000**, *39*, 85–97.
- (66) Whitmire, K. H.; Hutchison, J. C.; McKnight, A. L.; Jones, C. M. *J. Chem. Soc., Chem. Commun.* **1992**, 1021–1022.
- (67) Whitmire, K. H.; Jones, C. M.; Burkart, M. D.; Hutchison, J. C.; McKnight, A. *Mater. Res. Soc. Symp. Proc.* **1992**, *271*, 149–154.
- (68) Casely, I. J.; Ziller, J. W.; Mincher, B. J.; Evans, W. J. *Inorg. Chem.* **2011**, *50*, 1513–1520.
- (69) Evans, W. J.; Hain, J. H., Jr.; Ziller, J. W. *J. Chem. Soc., Chem. Commun.* **1989**, 1628–1629.
- (70) Chauhan, H. P. S.; Singh, R. K.; Kori, K. *Main Group Met. Chem.* **2002**, *25*, 511–516.
- (71) Clegg, W.; Norman, N. C.; Pickett, N. L. *Polyhedron* **1993**, *12*, 1251–1252.
- (72) Edelmann, F. T.; Noltemeyer, M.; Haiduc, I.; Silvestru, C.; Ceac-Olivares, R. *Polyhedron* **1994**, *13*, 547–552.
- (73) Lai, C. S.; Tiekink, E. R. T. Z. *Kristallogr.* **2007**, *222*, 532–538.
- (74) Mann, K. R.; Lewis, N. S.; Williams, R. M.; Gray, H. B.; Gordon, J. G. *Inorg. Chem.* **1978**, *17*, 828–834.
- (75) Curioni, A.; Andreoni, W. *J. Am. Chem. Soc.* **1999**, *121*, 8216–8220.
- (76) Humbs, W.; van Veldhoven, E.; Zhang, H.; Glasbeek, M. *Chem. Phys. Lett.* **1999**, *304*, 10–18.
- (77) Bhatnagar, D. C.; Forster, L. S. *Spectrochim. Acta* **1965**, *21*, 1803–1807.
- (78) Misra, A.; Kumar, P.; Kumar, L.; Dhawan, S. K.; Kamalasanan, M. N.; Chandra, S. *Indian J. Eng. Mater. Sci.* **2006**, *12*, 357–361.
- (79) Hopkins, T. A.; Meerholz, K.; Shaheen, S.; Anderson, M. L.; Schmidt, A.; Kippelen, B.; Padias, A. B.; Hall, H. K.; Peyghambarian, N.; Armstrong, N. R. *Chem. Mater.* **1996**, *8*, 344–351.
- (80) Niedermair, F.; Kwon, O.; Zojer, K.; Kappaun, S.; Trimmel, G.; Mereiter, K.; Slugovc, C. *Dalton Trans.* **2008**, 4006–4014.
- (81) Tsaryuk, V.; Zhuravlev, K.; Zolin, V.; Gawryszewska, P.; Legendziewicz, J.; Kudryashova, V.; Pekareva, I. *J. Photochem. Photobiol. A* **2006**, *177*, 314–323.
- (82) Qin, Y.; Pagba, C.; Piotrowiak, P.; Jäkle, F. *J. Am. Chem. Soc.* **2004**, *126*, 7015–7018.
- (83) Royer, J. E.; Zhang, C.; Kummel, A. C.; Trogler, W. C. *Langmuir* **2012**, *28*, 6192–6200.